JOURNAL OF APPLIED ELECTROCHEMISTRY 14 (1984) 329–340

Electrochemical characteristics of the lithium/carbon monofluoride battery and its component half-cells

JAMES R. SANDIFER, MARY R. SUCHANSKI

Research Laboratories, Eastman Kodak Company, Rochester, New York 14650, USA

Received 5 May 1983; revised 16 August 1983

The impedance spectrum of the Matsushita lithium/carbon monofluoride battery was studied extensively as a function of load, temperature, state of charge, and time after discharge. Resolution of the battery impedance spectrum into frequency domains characteristic of the electrolyte, the anode, and the cathode permitted the polarization and kinetic parameters of the individual battery electrodes to be measured. Most of the battery voltage loss is attributed to the carbon monofluoride cathode. Comparisons of the interfacial electrochemical properties of lithium half-cells in the battery electrolyte (1.0 mol dm^{-3} $LiBF_4$/γ-butyrolactone) with those of the *in situ* battery anode show that the battery anode is coated with a film. Attempts to correlate the high-frequency (> 1 Hz) parameters of the battery impedance with state of charge proved unsuccessful.

1. Introduction

The impedance technique is a valuable tool in the study of electrical storage cells and their component half-cells [1]. Analyses of battery impedance spectra permit identification and measurement of the ohmic and faradaic impedances in the battery and can provide kinetic, mechanistic, and structural (i.e. surface area and porosity) information about the individual battery electrodes [1]. This knowledge is important in assessing the contribution of individual cell components to the battery voltage losses under load, in determining the rate-limiting step in the overall battery reaction sequence, and in identifying battery failure modes. For aqueous battery chemistries with zinc anodes–Leclanché [2–4], alkaline zinc/manganese dioxide [5], and alkaline zinc/mercuric oxide [6] – it has been shown via the impedance technique that charge transfer and diffusion at the zinc anode are the rate-controlling processes in these battery systems. The impedance of the manganese dioxide electrode must also be considered in the alkaline zinc/manganese dioxide cell after ~ 20% of the charge has been removed [5]. In the lead-acid system, impedance measurements were used to determine the effect of lead alloy composition on the charge transfer and diffusional impedances of the lead oxide (PbO_2) layer formed on lead alloys [7], as well as the effect of lead alloy composition on the pore structure and the kinetic behaviour of reduced PbO_2 layers [8]. Recently, batteries containing organic electrolytes have been investigated by the impedance technique [9–11]. Important information concerning the conditions under which lithium film growth is enhanced or retarded in thionyl chloride was obtained from these studies [9, 10]. The charge-transfer kinetics of Li/LiBr in acetonitrile have also been characterized [11].

In certain instances impedance data have been used to monitor the amount of charge remaining in storage cells. Successful state-of-charge determinations by the impedance technique have been developed for the nickel–cadmium battery [12], the Leclanché battery [13], and the zinc/mercuric oxide battery [14]. Attempts to monitor the state of charge via impedance measurements of alkaline zinc/manganese dioxide cells [15] and secondary lead–acid cells [16] were less successful because variations of the impedance parameters with state of charge were either too small or parabolic. A state-of-charge test for the lithium/copper oxide cell based on the lithium activation resistance has been reported [17, 18] over a limited range of charge (100–90%), but the test can only be per-

0021-891X/84 $03.00 + .12 © 1984 Chapman and Hall Ltd.

formed 24 h after discharge. After the 24 h stabilization time the activation resistance continues to change and therefore cannot be used to monitor the state-of-charge. Hughes *et al.* [11] indicate that a state-of-charge measurement may be possible for the lithium/sulphur dioxide system, but unfortunately, they did not investigate time-after-discharge dependence.

We have investigated the impedance characteristics of the Matsushita lithium/carbon monofluoride battery [19] from the standpoint of both battery electrode kinetics and state of charge. Battery impedance data as functions of temperature, load, state of charge, and time after discharge are presented. Comparative experiments with lithium half-cells confirmed that the battery impedance spectrum can be resolved, according to frequency, into regions which are characteristic of the electrolyte, the anode, and the cathode. Selected frequency impedance measurements under load permitted battery polarization losses to be apportioned between the anode and the cathode and the kinetic parameters of the individual battery electrodes to be determined. Further information about the electrochemical properties of the lithium electrode in the battery electrolyte (1.0 mol dm^{-3} $LiBF_4$/γ-butyrolactone) was obtained from impedance measurements and d.c. polarization experiments on lithium half-cells. Some insights into the relationship between lithium electrode capacitances and the anode-film/electrolyte interface are presented. Comparison of the kinetic parameters of the lithium half-cells with those of the battery anode show that a film exists on the battery anode owing to its interaction with atmospheric and/or electrolyte components.

2. Theory

The battery impedance may be represented by the equivalent circuit shown in Fig. 1, which is essentially the Randles equivalent circuit discussed in great detail by Sluyters-Rehback and Sluyters [20]. V_{oc} represents the open-circuit or ideal voltage source of the battery, R_s is its total series resistance (solution plus separator), C_{dl} is the double-layer capacitance of one of the electrodes, R_{act} is the activation resistance of that electrode, and W is the diffusional polarization (Warburg) impedance of the battery. A more general circuit would contain additional elements to include the other electrode and the package itself. However, in the work reported here, the circuit shown in Fig. 1 was adequate for the interpretation of the data, although it required two modifications. First, the Warburg or diffusional polarization element was so highly conductive at frequencies between 1 and 10^3 Hz that it could be neglected. The circuit then reduces to a simple resistor/capacitor parallel combination in series with a resistor. Second, the mathematical representation of the impedance Z of such a circuit should be given by Equation 1

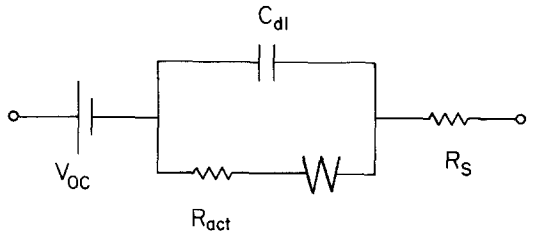

Fig. 1. Equivalent circuit representation of battery impedance.

$$Z = R_s + \frac{R_{act}}{1 + j\omega R_{act} C_{dl}} \quad (1)$$

where $j = (-1)^{1/2}$ and ω is the radial frequency. However, the data were more consistent with Equation 2

$$Z = R_s + \frac{R_{act}}{1 + (j\omega R_{act} C_{dl})^{\alpha}} \quad (2)$$

which includes the empirical parameter α. The Argand plot of Equation 2 (Fig. 2) is a lowered semicircle with its centre below the real axis. Notice that the centre of the semicircle would be on the real axis ($\theta = \pi/2$) if $\alpha = 1$, and Equation 2 would reduce to Equation 1.

Argand or Cole–Cole [21] plots which have lowered semicircles have been observed in a variety of cases including dielectrics [22], glass electrodes [23], and even biological membranes [24]. They are possibly caused by porosity or surface roughness effects [25, 26].

Equation 2 implies an equivalent circuit with a continuous distribution of relaxation times [27]. Such a circuit would consist of an infinite series of resistor/capacitor (RC) parallel combinations, each with a different RC time constant. The data pre-

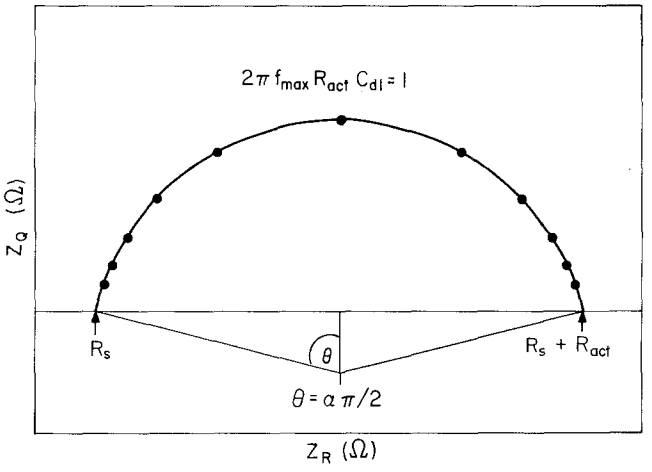

Fig. 2. Argand representation of Equation 2.

sented here could possibly be resolved into a finite series of such elements and still be consistent with Equation 2, within experimental error. However, resolution in most cases would have been extremely difficult, owing to close agreement between the data and this empirical expression.

The kinetic parameters of the battery electrodes were determined from relationships derived directly from the Butler–Volmer equation for a one-step one-electron transfer reaction [28]. The exchange current density i_0 of the lithium electrode was calculated from the slope of the current–voltage curves at low overpotentials, where the following linear relationship between the current and the overpotential η is theoretically predicted [29]

$$\left(\frac{\partial \eta}{\partial i}\right)_{C_{Li^+},T} = \frac{RT}{Fi_0} = R_{act} \qquad (3)$$

At higher overpotentials the exchange current density was determined from the intercept of $\ln i_a$ versus η plots, where i_a is the anodic portion of the total current density i ($i_a \simeq i$ at high overpotentials).

$$\ln i_a = \ln i_0 + (1-\beta)F\eta/RT \qquad (4)$$

The anodic transfer coefficient $(1-\beta)$ was obtained from the following relationship for a one-step electron transfer.

$$\left(\frac{\partial \ln i_a}{\partial \eta}\right)_{C_{Li^+},T} = (1-\beta)F/RT \qquad (5)$$

An equation similar to Equation 5 was used to calculate the cathodic transfer coefficient of the CF electrode.

3. Experimental

3.1. *Materials and cells*

The lithium/carbon monofluoride batteries were standard 2/3 A size (4300 coulombs rated capacity at 60 ohms load) with a jelly-roll configuration and were manufactured by Matsushita Electric of Japan. The electrolyte in these batteries was 1.0 mol dm^{-3} $LiBF_4$ in γ-butyrolactone (BL).

The cells used to measure the lithium impedance consisted of two lithium electrodes – a 1 cm^2 electrode and an 11 cm^2 counterelectrode. Both of the electrodes were lithium to ensure that the a.c. response of the cell was representative of lithium only. The electrodes were made by hammering lithium foil (Kawecki Berylco Industries, 0.019% Na) onto a 0.0127 cm thick titanium grid. The 1 cm^2 electrode was wrapped in one layer of Panasonic B separator (nonwoven polypropylene fabric, 0.0089 cm per layer) and placed adjacent to the counterelectrode. The electrodes were inserted into a Kapak plastic pouch, electrolyte was added to the pouch, and the pouch was sealed around the titanium grid tabs with a heat sealer.

A cylindrical glass cell was used to measure the lithium polarization. A side arm for the reference electrode was connected to the main body of the cell through small-bore glass tubing which served as a Luggin probe. The surface of the lithium working electrode was positioned close to the tip

of the Luggin probe to minimize the uncompensated ohmic resistance between the working electrode and the reference electrode. The working electrode and the reference electrode were both made from special-purity, 0.318 cm lithium rod (Lithium Corp. of America, 0.007% Na). The lithium rod was compression fitted into an electrode holder that consisted of a Teflon or polypropylene sleeve fitted tightly around a 0.318 cm titanium rod. The surface of the lithium rod was scraped clean with a razor blade and was subsequently polished with crocus cloth. The auxiliary electrode was a platinum-gauze cylinder.

The electrolyte was 1.0 mol dm^{-3} $LiBF_4$ in γ-butyrolactone. Aldrich Gold Label γ-butyrolactone was vacuum distilled once over activated type-5A molecular sieves at 50–55° C (1.5–2 mm Hg). The solvent purity, determined by gas chromatographic (GC) analysis on a Poropak Q column, was > 99%. The $LiBF_4$ was obtained from Foote Mineral Company (estimated purity 97.5%) and was purified by reprecipitation from 4:1 methylene chloride/acetone. The reprecipitated material typically contained 0.1% water and no detectable LiF (a major contaminant in $LiBF_4$) as evidenced by the clarity of its organic solutions.

All cell assembly and electrolyte preparations took place in a Vacuum Atmospheres dry box, which maintains a water-, O_2-, and N_2-free atmosphere (O_2 typically < 10 ppm).

3.2. *A.c. techniques*

The response of Li/CF batteries and lithium electrodes to small-amplitude, sine-wave excitation was measured as follows. A Hewlett-Packard Model 203A function generator was used to generate a < 5 mV (average) signal with frequencies between 5.63 mHz and 1 kHz. The sine-wave excitation signal was applied to the electrochemical cell through a PAR 173 potentiostat which controlled the d.c. potential of the cell. Measurements at zero current were made by adjusting the potentiostat voltage to equal the open-circuit cell voltage ('null' mode of the potentiostat) before applying the voltage to the cell. Current flow through the cell resulting from the a.c. and d.c. applied signals was converted to a voltage by a PAR 176 current-to-voltage converter. The modulus of the current, or more properly the transduced voltage, was resolved into real and quadrature admittance components by use of a cross-correlation circuit described in the literature [30]. Above 1 Hz this instrument provides a direct reading of the real or quadrature admittance. Below 1 Hz a gated integrator is used. The admittance values were mathematically converted into the real and quadrature impedance values for preparing Argand plots [20].

The temperature dependence of the battery impedance spectrum was measured primarily at the open-circuit battery voltage because, under load, there was considerable drift in the direct current. Temperature at 35° C and above was controlled by immersing the battery in a Haake FS2 constant-temperature bath filled with silicon oil. Below 35° C the temperatures reported are ambient (~ 23° C).

Batteries with various amounts of charge removed were prepared by discharging them through a 6 Ω load for different periods of time. The impedance spectra of these batteries were then measured at their open-circuit voltages at times varying from two days to 15 months after discharge.

Selected frequency impedance measurements of the commercial battery under load were made by applying a known voltage to the battery via the PAR potentiostat and monitoring the resultant current flow on either a Hewlett-Packard 3465A digital multimeter or a Houston Instrument Omniscribe recorder. The alternating voltage was applied to the battery only after steady-state current flow was achieved. It was sometimes difficult to achieve steady state because at high loads (applied voltages much less than the open-circuit voltage) the current drifted upward owing to heating of the battery, whereas at low loads the current drifted downward owing to the very slow approach to steady state. Hence a considerable amount of charge had to be withdrawn from the battery (up to 25% of the rated capacity) to obtain polarization data over a wide range of currents. However, kinetic information obtained from these selected frequency impedance measurements is considered valid because of the essentially flat discharge curve of Li/CF batteries [19].

3.3. *Galvanostatic polarization*

Galvanostatic polarization of the lithium electrode

was accomplished with a PAR model 173 potentiostat/galvanostat. The uncompensated ohmic resistance between the working electrode and the tip of the Luggin probe was not corrected for, as we felt that the cell geometry would minimize the IR solution drop. To prevent air and moisture contamination of the cell contents and to provide electrolyte agitation, ultra high purity argon (99.999%) was continuously bubbled through the cell during measurement. The electrolyte was sampled for water content both before and after the polarization runs and typically contained 100–300 ppm H_2O. Precise temperature control of the electrolyte was maintained by circulating ethylene glycol from a thermostatted bath through a dish in which the cell was positioned. A Neslab Model TE10 circulating thermostat was used in conjunction with a Neslab Model PBC-2 bath cooler for this purpose.

4. Results and discussion

4.1. *Impedance characteristics of commercial batteries*

A typical Argand plot is shown in Fig. 3. Above frequencies of 1 Hz the data are adequately represented by an equivalent circuit which consists of a resistance in series with a parallel combination of an activation resistance and a double-layer capacitance (i.e. the equivalent circuit in Fig. 1 without the Warburg impedance). Equation 2 provides an accurate fit to the high-frequency impedance data, as the centre of the semicircle drawn through the data is below the real axis. As will be shown in Section 4.2, the high-frequency arc can be assigned to the lithium anode, and the low-frequency data (< 1 Hz) are associated with the carbon monofluoride cathode.

The temperature dependences of the impedance

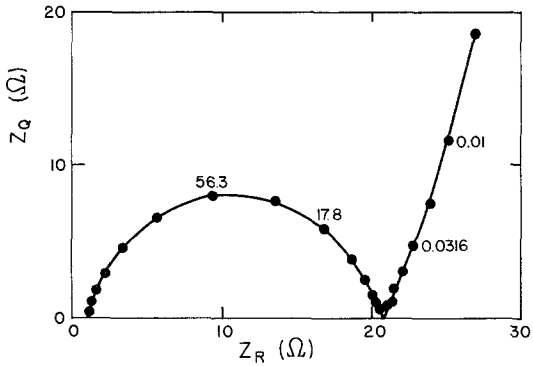

Fig. 3. Argand diagram of a Li/CF battery.

parameters in Equation 2 are shown in Table 1. Resistance values could usually be determined to within 0.1 Ω except in certain instances in which the frequency range did not completely define an arc. The parameters C_{dl} and α are accurate to one significant figure. For subsequent comparison, Table 1 includes values of the exchange current density which are related to R_{act} by Equation 3. The active area of the lithium electrode in the commercial battery is 50.6 cm^2, and the exchange current density has been calculated with this area.

The data in Table 1 show that only R_{act} (and therefore i_0) is strongly temperature dependent. The fact that R_s, which is primarily associated with the electrolyte resistivity, is not strongly temperature dependent probably reflects the low activation energy for conductance. For example, the activation energy for conductance of a 1 mol dm^{-3} $LiAlCl_4$–$SOCl_2$ solution has been calculated to be 0.588 kcal/mol [31]. Over the 33° C temperature range in Table 1 this value of activation energy would cause R_s to change by only 75 mΩ. A plot of ln R_{act} versus $1/T$ is linear ($R_{corr} = 0.998$), and from the slope of this plot an activation energy E_A of 16 kcal/mol was obtained. We observed that the history of the battery can affect the activation energy. Specifically, if a bat-

Table 1. Impedance parameters of Li/CF batteries – temperature dependence

T (° C)	R_s (Ω)	R_{act} (Ω)	C_{dl} (μF)	α	i_0 ($mA\ cm^{-2}$)
22	0.7	~ 14.0	~ 200	0.93	0.036
35	0.7	4.9	240	0.91	0.11
45	0.7	2.0	250	0.93	0.27
55	0.7	0.9	–	0.93	0.62

$E_A = 16.1$ kcal mol^{-1}

*Table 2. Impedance parameters of Li/CF Battery – temperature dependence of partly discharged battery**

T (° C)	R_s (Ω)	R_{act} (Ω)	C_{dl} (μF)	α	i_0 ($mA\ cm^{-2}$)
22	0.8	37.7	420	0.86	0.014
37	0.7	6.7	180	0.90	0.08
45	0.7	2.5	360	0.90	0.22
55	0.7	0.9	–	0.90	0.63
$E_A = 21.8$ kcal mol^{-1}					
Parameters remeasured 4 days later					
23	0.7	18.6	270	0.87	0.027
37	0.7	4.7	250	0.87	0.11
45	0.7	2.4	280	0.87	0.23
55	0.7	1.0	280	0.87	0.57
$E_A = 17.6$ kcal mol^{-1}					

* 1.2 kC removed.

tery has been drained, the temperature dependence of R_{act} can vary with the time elapsed after drainage. Table 2 compares the temperature dependence of the impedance parameters of a partly discharged battery (~ 1200 C of a total of 4300 C) which were measured several hours versus four days after general testing under resistive loads. The activation energy E_A fell from 21.8 to 17.6 kcal/mol within this time. This suggests that the charge-transfer characteristics of the lithium electrode are altered by current flow across the electrode/electrolyte interface.

The high-frequency impedance parameters of the Li/CF battery (R_s, R_{act}, C_{dl}, and α) were extensively monitored as a function of both the number of coulombs withdrawn from the cell and the time after discharge. Of the four parameters, only R_{act} showed significant variations with the amount of charge removed. Fig. 4 shows the variation in R_{act} versus the coulombs removed for a series of partly discharged batteries at various times after discharge. At any particular time after discharge the R_{act} values oscillate considerably as a function of the charge withdrawn: maximum variations in R_{act} of ~ 18 Ω at two days after discharge to ~ 48 Ω at 86 days after discharge. These oscillations are real and do not reflect innate battery-to-battery variations, since the average R_{act} of three fresh batteries from the same lot, measured on different days, was 23 ± 1.2 Ω. Similar observations have been reported before. See Tables 1 and 2 and Fig. 3 of [18] for example. The general trend of increasing R_{act} with time after discharge for a battery at a particular state of charge suggests lithium film formation caused by the interaction of lithium with the electrolyte or an electrolyte contaminant. It is possible that discharging the lithium electrode disrupts a protective anode film and thus exposes an active lithium surface which can react with an electrolyte component to form another film. The growth of such protective films on lithium has been observed in propylene carbonate, tetrahydrofuran, thionyl chloride ($SOCl_2$), and SO_2 electrolytes [32, 33]. The manner in which R_{act} varies with the coulombs removed and the time after discharge precludes the use of these data to measure the state of charge in commercial batteries.

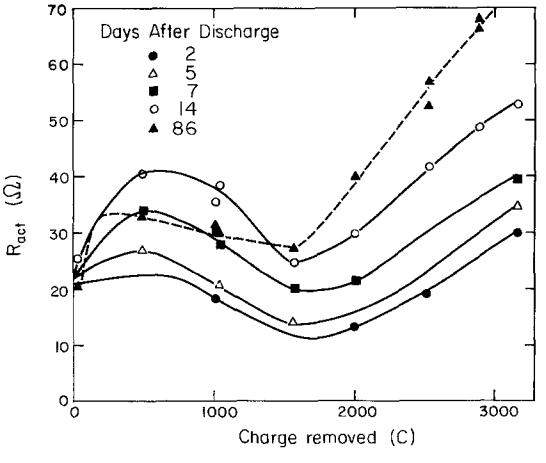

Fig. 4. Dependence of R_{act} on state of charge.

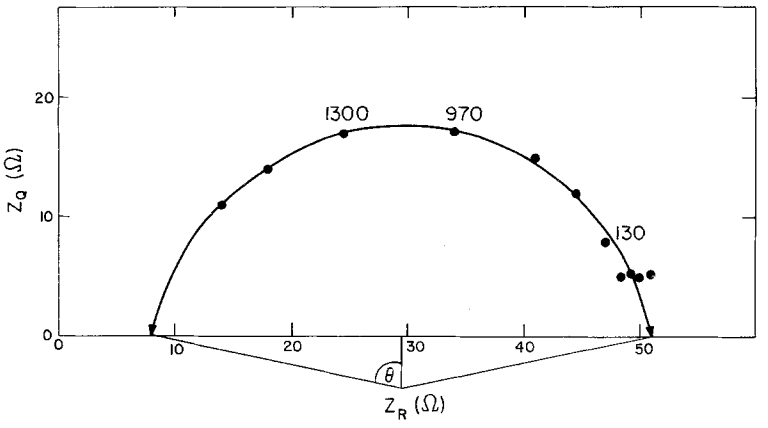

Fig. 5. Argand diagram of a freshly prepared lithium half-cell in 1.0 mol dm^{-3} $LiBF_4/\gamma$-BL at room temperature.

4.2. *Impedance of lithium half-cells*

The impedance of lithium half-cells was studied in an attempt to correlate their impedance with the high-frequency battery impedance. The high-frequency Argand plot of a freshly prepared lithium half-cell (Fig. 5) is a lowered semicircle with $\alpha = 0.88$ and resembles the high-frequency arc of the battery impedance diagram shown in Fig. 1 ($\alpha = \sim 0.9$). Table 3 compares the impedance parameters (R_s, R_{act}, C_{dl}, α, and i_0) of the lithium half-cells as functions of time after cell preparation and storage conditions. R_{act} of the freshly prepared lithium half-cell, when compared for equal electrode areas (50.6 cm^2), is a factor of 26 smaller than that of a fresh battery (0.87 versus 23 Ω). The respective exchange current densities are 0.59 mA cm^{-2} for the lithium half-cell and 0.022 mA cm^{-2} for fresh batteries. After one-week storage of the lithium half-cell in the dry box, with intermittent exposure to air, the R_{act} of the half-cell is within a factor of three of typical battery values. Rigorous exclusion of air and moisture from the half-cells retards but does not halt the growth of R_{act} with time, as is shown for the half-cell stored for one week in the dry box. These data suggest that the lithium anode can undergo film formation by reacting with atmospheric components (air, H_2O) and components in the $LiBF_4/\gamma$-butyrolactone electrolyte. It is likely that the lithium anode in the battery formed a film during the manufacturing process and during subsequent storage. The double-layer capacitances of the lithium half-cells (150–200 μF when corrected to the area of the anode in the battery) agree well with the values reported for batteries in Tables 1 and 2. Thus, on the basis of the above comparisons between the high-frequency, lithium half-cell impedance data and the battery impedance data, it is concluded that the high-frequency arc of the battery corresponds to the lithium anode. Furthermore, as the low-frequency (< 13 Hz) impedance of the lithium half-cell (not shown in Fig. 5) does not have the capacitive component observed in the battery impedance diagram in Fig. 3, the low-frequency portion of the battery impedance is assigned primarily to the carbon monofluoride cathode.

Table 3. Impedance parameters of lithium half-cells at room temperature

R_s (Ω)	R_{act} (Ω)	C_{dl} (μF)	α	i_0 ($mA\ cm^{-2}$)
7.8*	43.8	3.8	0.88	0.59
10.0†	468	2.6	0.78	0.055
7.5‡	103	4.0	0.86	0.25

* Fresh cell.
† After one week of intermittent exposure to air.
‡ Stored in dry box for one week.

On the basis of the double-layer capacitance values in Table 3, some speculation about the nature of the lithium anode/electrolyte interface can be made. If the double-layer capacitance is associated primarily with the ions in solution at the electrode/electrolyte interface, and if it is further assumed that the activation resistance is inversely proportional to the effective 'electrochemical' area of the electrode, then the product of R_{act} and C_{dl} should be constant. Clearly this is not the case; a tenfold increase in R_{act} results in only a 30% decrease in C_{dl}. It is possible that other

types of capacitance dominate the measured values Peled [34] has suggested that in some nonaqueous battery systems the alkali metal is covered by a solid electrolyte which acts as an interphase between the metal and the solution. In these instances the electrode–electrolyte properties, including the kinetic parameters and the double-layer capacitance, will be controlled by the solid-electrolyte interphase (SEI). Electrodes with double-layer capacitances of less than $5\,\mu F\,cm^{-2}$ are considered candidates for the SEI model [34]. An example of a nonaqueous electrolyte system in which lithium is believed to have a solid electrolyte coating is the $LiClO_4$/propylene carbonate (PC) electrolyte [35]. Scarr [36] measured double-layer capacitances of $2.4–5.2\,\mu F\,cm^{-2}$ for this system. Since the double-layer capacitances reported in Table 3 are similar to those reported for lithium in $LiClO_4$/PC, and as the kinetic parameters of lithium in both these electrolyte systems are similar (see Section 4.3), it is likely that the lithium film in $LiBF_4/\gamma$-BL is similar to that in $LiClO_4$/PC. Hence a solid electrolyte interphase may possibly control the anode's electrochemical behaviour.

Hughes *et al.* [11] report similar values for the double-layer capacitance of lithium in $LiBr/CH_3CN$ but interpret their results in terms of a pitting mechanism. Variations in the $R_{act}C_{dl}$ product are then caused by changes in the concentration of lithium ions, which affects R_{act} but not C_{dl}.

4.3. *Polarization of commercial batteries*

Further characterization of Li/CF battery electrode kinetics was carried out by d.c. polarization of the battery coupled with selected frequency impedance measurements. These measurements also permitted separation of the anode and cathode polarization losses from the total battery polarization. As shown in Fig. 3, the frequency response of the CF cathode is different from that of the lithium anode; frequencies of > 1 Hz reflect only the series resistance R_s and the lithium activation resistance R_{act}, whereas frequencies < 1 Hz are characteristic of the cathode. At frequencies between 1 and 10 Hz, Y_R, the real component of the admittance, is very nearly equal to $(R_s + R_{act})^{-1}$, with the maximum error estimated to be 0.4%. Therefore to separate the anode polarization and ohmic losses from the cathode polarization, the room-temperature complex admittance of a Li/CF battery was measured at 10 Hz while voltages from 3.0 to 2.2 V were applied in 0.1 V increments. The admittance values were recorded after steady-state currents were achieved (from 15 min at 2.2 V to 22h at 3.0 V). The ohmic loss at each of the applied voltages was calculated by multiplying the corresponding steady-state current by R_s ($\sim 0.7\,\Omega$). Voltage drops across R_{act} were estimated by numerically evaluating the integral $\int_0^I R_{act}\,dI$, where I is the direct current. The remaining portion of the difference between the open-circuit voltage (3.414 V) and the load voltage was assigned to the cathode. The results of these calculations are shown in Fig. 6 in the form of Tafel plots (V versus $\ln I$).

The kinetic parameters [i_0 and $(1-\beta)$] of the lithium anode were determined by treating the anode polarization data in the linear portion of the

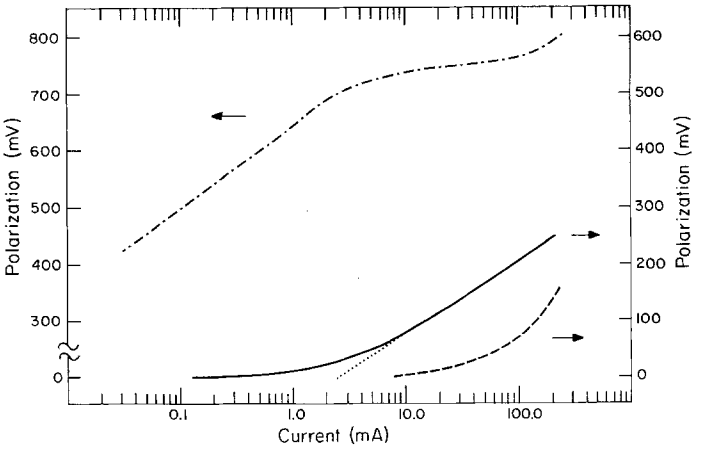

Fig. 6. Polarization losses of Li/CF battery: cathode polarization (·····), anode polarization (——), ohmic losses (----).

V versus $\ln I$ plot in Fig. 6 by the Allen–Hickling method [37], in which the total current I is corrected for the backward reaction current. The current for the reaction of interest, in this case the anodic dissolution of lithium, is given by the expression $I/[1 - \exp(-F\eta/RT)]$. From Equation 4, a value of 0.049 mA cm^{-2} was obtained for the exchange current density and a value of 0.46 for the anodic transfer coefficient. The i_0 value is greater than the room-temperature i_0 values of 0.014–0.036 mA cm^{-2} determined from the open-circuit impedance data in Tables 1 and 2. This may be the result of internal heating of the battery or of partial disruption of the anode film during the polarization experiments. The data in Fig. 6 also indicate that the contribution of the battery anode polarization to the total battery polarization is small (~ 20%).

In contrast, Fig. 6 shows that the CF cathode contributes the major portion of the battery polarization (414 mV at an applied voltage of 3.0 V to 798 mV at an applied voltage of 2.2 V). From applied voltages of 3.0 to 2.7 V the plot of cathode polarization versus the logarithm of the current is linear with a Tafel slope of 155 mV per decade and a cathodic transfer coefficient of 0.38. These values agree remarkably well with CF half-cell polarization data [38]. Below 2.7 V the cathode polarization data no longer follow straight-line behaviour. This is most likely due to internal battery heating, as the CF cathode polarization is strongly temperature dependent [39].

4.4. *D.c. polarization of lithium half-cells*

Temperature-dependent micropolarization data for 'fresh' lithium anodes in 1.0 mol dm^{-3} $LiBF_4$/γ-BL solution are shown in Table 4. The exchange current density i_0 was calculated from the slopes of the current–voltage curves as defined in Equation 3. The activation energy E_A of the lithium electrode was calculated from the slope of the plot of $\ln i_0$ versus $1/T$. The values of i_0 represent the average of five separate determinations at each temperature, and the activation energy is the average value from six sets of experimental data.

Table 4. The variation of i_0 with temperature for the Li electrode in 1.0 mol dm^{-3} $LiBF_4$/γ-BL

Temperature (° C)	i_0 *(mA* cm^{-2}*)*
10	0.50 ± 0.15
25	1.57 ± 0.11
40	3.77 ± 1.11
$E_A = 11.8 \pm 0.5$ kcal mol^{-1}	

Comparison of the micropolarization data in Table 4 with the impedance data in Table 3 reveals an approximately threefold difference in the room temperature i_0 values of fresh lithium half-cells. This is most probably explained by the different experimental procedures followed for the two measurements. In the micropolarization experiments, the lithium electrode surface was scraped with a razor blade before immersion in the electrolyte, and the measurements were made within 1 h of cell preparation. For the impedance experiments the lithium foil was used 'as received', and the time between cell preparation and measurement was as long as 24 h. Therefore the data reported in Table 4 are considered to represent more closely a 'film-free' lithium electrode. These values are in reasonable agreement with those measured in the more commonly studied electrolyte system $LiClO_4$/PC. For example, from current interruptor studies, Scarr [36] obtained an i_0 value of 1.78 ± 0.33 mA cm^{-2} at 23° C for a 'film-free' lithium electrode in 1.0 mol dm^{-3} $LiClO_4$/PC. Meibuhr [40] reported a value of 0.95 ± 0.5 mA cm^{-2} at 28° C in 1.0 mol dm^{-3} $LiClO_4$/PC. Hughes *et al.* [11] reported 0.7 mA cm^{-2} in 2.35 mol dm^{-3} $LiBr/CH_3CN$. The E_A value of 11.8 ± 0.5 kcal mol^{-1} compares with a value of 8.5 ± 0.3 kcal mol^{-1} for a lithium electrode in 1.0 mol dm^{-3} $LiClO_4$/PC [40].

Further kinetic data for 'fresh' lithium anodes in 1.0 mol dm^{-3} $LiBF_4$/γ-BL were obtained from half-cell polarization data obtained at higher currents. Fig. 7 shows an Allen–Hickling plot of the data in which the anode overpotential η is plotted versus the current density for anodic dissolution i_a. The anodic transfer coefficient $(1 - \beta)$ was found to be 0.31 ± 0.04 from the polarization data taken when the current was successively increased, whereas the average value of $(1 - \beta)$ calculated from the reverse polarization runs was 0.55 ± 0.002. In $LiClO_4$/PC electrolyte, Scarr [36] obtained a $(1 - \beta)$ value of 0.62, and Meibuhr [40] obtained 0.67. Thus, although the activation energies and i_0 values of 'clean' lithium anodes are

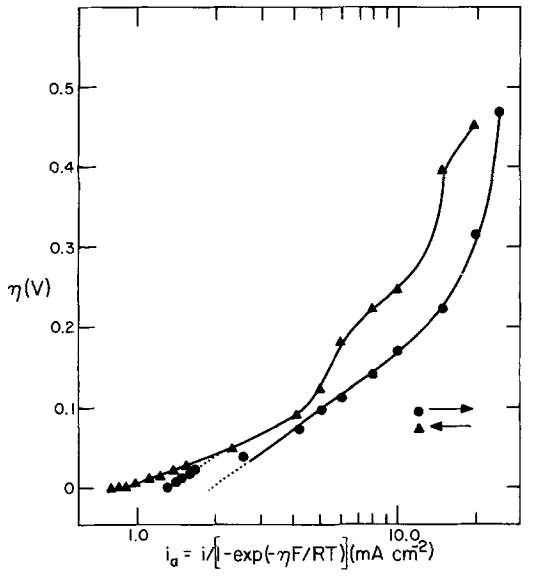

Fig. 7. Allen–Hickling plot of lithium polarization data: 1.0 mol dm^{-3} $LiBF_4$, 25° C.

similar in $LiBF_4$/BL and $LiClO_4$/PC electrolytes, the lithium anodic transfer coefficient differs significantly in these two electrolyte systems. Hughes *et al.* [11] reported $(1-\beta)$ equal to 0.63 in CH_3CN, indicating that the $LiBF_4$/γ-BL system might be a unique case.

Two features of the Allen–Hickling plot deserve comment. First, for the data obtained while the current was increased there are two distinct regions of linearity which have the same slopes but different x-axis intercepts: one below and one above current densities of 2 mA cm^{-2}. This type of behaviour was reported by Scarr [36] for $LiClO_4$/PC solutions and was explained by the electrochemical removal at the higher current densities of an insulating film on the lithium electrode surface. Second, a large hysteresis is observed between the data taken upon increasing and decreasing the current. At the higher current densities (> 5 mA cm^{-2}) this may have resulted from gassing at the electrode surface. Below 5 mA cm^{-2} the smaller slope and x-axis intercept (exchange current density) for the reverse polarization data suggest that over the 2 h experiment the lithium surface had reacted with electrolyte contaminants (air, moisture).

4.5. *Comparison of Li half-cell and battery kinetic parameters*

Table 5 affords a direct comparison of the kinetic parameters of the lithium anode in lithium half-cells and in the Li/CF battery as determined by open-circuit impedance measurements and d.c. polarization experiments. In most cases the numbers reported in Table 5 are for 'fresh' Li half-cells and for batteries that had no coulombs removed before testing. Discrepancies between impedance and polarization data for the battery have been explained previously, as have the differences between the half-cell impedance and d.c. polarization data. The most striking contrast between battery and half-cell parameters was the factor of 10–30 difference in the exchange current density. This comparison strongly supports the conclusion that a film exists on the battery anode, owing either to atmospheric contamination or to interaction with the electrolyte and its impurities. Given the hypothesis that a film has grown on the battery anode, it is not surprising that the anodic transfer coefficient for the battery anode (0.46) was different from that of the 'fresh' lithium anode (0.31). The half-cell data provided evidence that the transfer

Table 5. Comparison of lithium anode kinetic parameters – battery versus half-cell

	*Battery**	*Battery†*	*Half-cell‡*	*Half-cell§*
i_0 (mA cm^{-2})¶	0.049	0.022	1.57	0.59
$(1-\beta)$¶	0.46	–	0.31	–
E_A (kcal mol^{-1})	–	16–22	11.8	–

* Polarization data.
† Open-circuit impedance data.
‡ Polarization data, 'fresh' lithium.
§ Open-circuit impedance data, 'fresh' lithium.
¶ Room-temperature values.

coefficient was dependent on the state of the lithium surface; half-cells that had reacted with the electrolyte for several hours had a transfer coefficient of 0.55, compared with 0.31 for the 'fresh' half-cell. Similarly, it is reasonable that the activation energy of the battery (16–22 kcal mol^{-1}) was greater than that of the lithium half-cell (11.8 kcal mol^{-1}) since the exchange current density and activation energy are exponentially related.

The data collected in Table 5 are important in that they provide fundamental information about the lithium electrode kinetics in organic electrolytes, but they also have practical significance. The impedance and polarization techniques could be used in battery manufacturing quality control to monitor the degree of lithium surface contamination. The impedance method is particularly attractive for this purpose in that an insignificant number of coulombs are withdrawn from the battery during testing.

5. Summary

The impedance spectrum of the Matsushita Li/CF battery was resolved into fequency domains characteristic of the electrolyte, the anode, and the cathode. The high-frequency arc was assigned to the lithium anode on the basis of lithium half-cell impedance data, and the low-frequency capacitive 'tail' was assigned to the cathode.

None of the high-frequency battery impedance parameters (R_s, R_{act}, C_{dl}) showed trends with coulombs removed that could be used to monitor the battery state of charge. Furthermore, the anode activation resistance R_{act} was unstable with respect to time after discharge.

The interfacial electrochemical properties of lithium in 1.0 mol dm^{-3} $LiBF_4$/γ-BL electrolyte were studied. The double-layer capacitances of lithium electrodes in this electrolyte (3–6 μF cm^{-2}) are characteristic of electrodes with solid-electrolyte interphases, as has been postulated for lithium and magnesium electrodes in thionyl chloride and lithium in $LiClO_4$/PC [34]. The exchange current density and activation energy of 'clean' lithium electrodes in $LiBF_4$/γ-BL are similar to those of lithium in $LiClO_4$/PC electrolyte.

The kinetic parameters of the battery anode and cathode were determined from load-dependent impedance measurements, and the battery anode activation energy was obtained by temperature dependent impedance measurements. The discrepancies between the battery anode values and those of clean lithium surfaces in 1.0 mol dm^{-3} $LiBF_4$/γ-BL electrolyte can be explained by film growth on the battery anode due to its interaction with water and other electrolyte components. In addition to providing kinetic parameters, the load-dependent impedance measurements permitted separation of the contributions of the anode, the cathode, and the electrolyte to the total battery polarization. The cathode losses account for most of the battery polarization.

Acknowledgements

We thank P. J. Hyk, M. A. Faust and N. N. Cornfield for performing many of the impedance experiments.

References

[1] N. A. Hampson, S. A. G. R. Karunathilaka and R. Leek, *J. Appl. Electrochem.* **10** (1980) 3.
[2] S. A. G. R. Karunathilaka, N. A. Hampson, R. Leek and T. J. Sinclair, *ibid.* **10** (1980) 357.
[3] *Idem, ibid.* **10** (1980) 603.
[4] M. Aslam and J. A. Harrison, *Electrochim. Acta* **26** (1981) 937.
[5] S. A. G. R. Karunathilaka, N. A. Hampson, R. Leek and T. J. Sinclair, *J. Appl. Electrochem.* **11** (1981) 715.
[6] S. A. G. R. Karunathilaka, N. A. Hampson, T. P. Haas, R. Leek and T. J. Sinclair, *ibid.* **11** (1981) 573.
[7] N. A. Hampson, S. Kelly and K. Peters, *ibid.* **11** (1981) 751.
[8] *Idem, ibid.* **11** (1981) 765.
[9] J. Phillips and H. F. Gibbard, Proceedings of the Symposium on Lithium Batteries, (edited by H. V. Venkatasetty) The Electrochemical Society, Princeton, New Jersey (1981).
[10] J. Phillips, J. C. Hall and H. F. Gibbard, *ibid.*
[11] M. Hughes, S. A. G. R. Karunathilaka, N. A. Hampson and T. J. Sinclair, *J. Appl. Electrochem.* **12** (1982) 537.
[12] S. Sathyanarayana, S. Venugopalan and M. L. Gopikanth, *ibid.* **9** (1979) 125.
[13] S. A. G. R. Karunathilaka, N. A. Hampson, R. Leek and T. J. Sinclair, *ibid.* **10** (1980) 799.
[14] J. J. Winter, J. T. Breslin, R. L. Ross, H. A. Leupold and F. Rothwarf, *J. Electrochem. Soc.* **122** (1975) 1434.
[15] S. A. G. R. Karunathilaka, N. A. Hampson, R. Leek and T. J. Sinclair, *J. Appl. Electrochem.* **11** (1981) 365.

[16] M. L. Gopikanth and S. Sathyanarayana, *ibid.* 9 (1979) 369.
[17] N. A. Hampson, S. A. G. R. Karunathilaka, R. Leek and T. J. Sinclair, *Surf. Technol.* 15 (1982) 101.
[18] S. A. G. R. Karunathilaka, R. Leek, N. A. Hampson, M. Hughes and T. J. Sinclair, *J. Appl. Electrochem.* **13** (1983) 351.
[19] M. Fukuda and T. Iijima, in 'Power Sources 5' (edited by D. H. Collins) Academic Press, New York (1975) Ch. 46.
[20] M. Sluyters-Rehbach and J. H. Sluyters, in 'Electroanalytical Chemistry', Vol. 4 (edited by A. J. Bard) Marcel Dekker, New York (1970) pp. 1–128.
[21] K. S. Cole and R. H. Cole, *J. Chem. Phys.* 9 (1941) 341.
[22] J. H. Kennedy, J. R. Akridge and M. Kleitz, *Electrochim. Acta* 24 (1979) 781.
[23] J. R. Sandifer and R. P. Buck, *J. Electroanal. Chem., Interfacial Electrochem.* 56 (1974) 385.
[24] K. S. Cole, 'Membranes, Ions and Impulses', University of California Press, Berkeley, California (1972).
[25] R. de Levie, *Adv. Electrochem.* 6 (1967) 329.
[26] H. Keiser, K. D. Beccu and M. A. Gutjahr, *Electrochim. Acta* 24 (1976) 539.
[27] R. Fuoss and S. G. Kirkwood, *J. Amer. Chem. Soc.* 63 (1941) 385.
[28] J. O'M. Bockris and A. K. N. Reddy, 'Modern Electrochemistry', 3rd edn., Plenum Press, New York (1977) p. 879.
[29] *Idem, ibid.*, p. 895.
[30] A. J. Bentz, J. R. Sandifer and R. P. Buck, *Anal. Chem.* 46 (1974) 543.
[31] H. V. Venkatasetty and D. J. Saathoff, *J. Electrochem. Soc.* 128 (1981) 773.
[32] A. N. Dey, *Electrochim. Acta* 21 (1976) 377.
[33] *Idem, Thin Solid Films* 43 (1977) 131.
[34] E. Peled, *J. Electrochem. Soc.* 126 (1979) 2047.
[35] Y. Geronov, F. Schwager and R. H. Muller, 'Proceedings of the Workshop on Lithium Non-aqueous Battery Electrochemistry', (edited by E. B. Yeager, B. Schumm, Jr, G. Blomgren, D. R. Blankenship, V. Leger and J. Akridge), The Electrochemical Society, Princeton, New Jersey (1980) pp. 115–29.
[36] R. F. Scarr, *J. Electrochem. Soc.* 117 (1970) 295.
[37] R. L. Allen and A. Hickling, *Trans. Faraday Soc.* 53 (1957) 1626.
[38] W. Tiedemann, *J. Electrochem. Soc.* 121 (1974) 1308.
[39] M. R. Suchanski and P. J. Muehlbauer, unpublished results.
[40] S. G. Meibuhr, *J. Electrochem. Soc.* 117 (1970) 56.